A complex corona between olivine and plagioclase from the Jotun Nappe, Norway, and the diffusion modelling of multimineralic layers

J. R. ASHWORTH, J. J. BIRDI*

School of Earth Sciences, University of Birmingham, Edgbaston, Birmingham B15 2TT, U.K.

AND

T. F. EMMETT

Geology Division, Anglia Polytechnic, East Road, Cambridge CB1 1PT, U.K.

Abstract

Coronas containing Ca-amphibole with aluminous minerals have been characterised optically and by scanning electron microscopy, analytical transmission electron microscopy and electron-probe microanalysis. The layers nearest to plagioclase are amphibole + epidote + kyanite, followed by amphibole + epidote + staurolite + spinel. These assemblages are consistent with water-undersaturated conditions, possibly at lower metamorphic grade than the commoner assemblage amphibole + spinel. Observed mineral proportions and compositions were used in a seven-layer model of steady-state, diffusion-controlled growth with local equilibrium. This model is not fully realistic, because the observed amphibole is strongly zoned from tschermakitic to actinolitic away from plagioclase, suggesting disequilibrium. However, the four-mineral layer has been successfully modelled assuming local equilibrium, with diffusion coefficients L_{ii} larger for i = FeO and MgO than for SiO_2, $AlO_{3/2}$, CaO and $FeO_{3/2}$. Retarded grain-boundary diffusion of the latter components is explicable by crystal-chemical effects. The number of minerals per layer is constrained by a modified form of the metasomatic phase rule of Korzhinskii, with the role of 'inert' components played by relatively immobile ones (having relatively small fluxes and relatively small diffusion coefficients).

KEYWORDS: coronas, kyanite, staurolite, tschermakitic amphibole, metasomatic phase rule.

Introduction

GROWTH of a mineralogically layered structure, accompanied by chemical transport through the layers, is exemplified on a small scale by coronas (reaction rims) formed between two reactant minerals. The theory of steady-state, diffusion-controlled growth developed by Joesten (1977) has been successfully extended to metamorphic coronas formed in open systems (Ashworth and Birdi, 1990; Johnson and Carlson, 1990). Hitherto, the maximum number of layers modelled in coronas was four (Grant, 1988; Johnson and Carlson, 1990), and the maximum number of minerals per layer was three (Carlson and Johnson, 1991; Ashworth *et al.*, 1992). In this paper, a complex corona between olivine (Ol; mineral abbreviations from Kretz, 1983) and plagioclase (Pl) is modelled in terms of seven layers, one of which contains four minerals. Modelling of the multimineralic layer was found to require immobile behaviour of components additional to $AlO_{3/2}$ and SiO_2, which had previously been identified as immobile in coronas containing two-mineral symplectites (Ashworth and Birdi, 1990; Ashworth *et al.*, 1992). This behaviour of the model can be compared instructively with the constraints on the number of mobile components in the classic theory of metasomatic equilibrium (Korzhinskii, 1959).

High mobility can be defined in different ways: large flux, small chemical-potential differences, or low kinetic barriers to transport. In diffusion theory, the transport definition (large diffusion coefficient) is fundamental, and large flux is likely. On the other hand, the theory used here

* Present address: 17 Stonedown Close, Bilston, Wolverhampton WV7 9YN, U.K.

Mineralogical Magazine, December 1992, Vol. 56, pp. 511–525

assumes local equilibrium at every point in gradients of chemical potential, μ, and a thermodynamic definition of mobility is relevant. The number of phases (minerals) in an assemblage (layer) may indicate a minimum number of relatively immobile components (Korzhinskii, 1959; Thompson, 1970). According to the classic theory of metasomatic reaction with local equilibrium (Korzhinskii, 1959), $\Phi \leqslant N_I$, where Φ is the number of 'determining inert' components. An inert component (which has spatially variable μ, controlled internally within a layer), is contrasted with a 'perfectly mobile' one, which is transported so easily that it has a constant μ value, imposed by the surroundings (Korzhinskii, 1959).

Diffusion theory quantitatively relates fluxes to μ-gradients, which may be finite for all components so that their simple classification into mobile and inert breaks down. For example, Frantz and Mao (1979), having computed various hypothetical layer sequences, emphasised that they found no relation between the number of phases per layer and the number of components having relatively small diffusion coefficients. Joesten (1991) has demonstrated the lack of a simple relationship between the number of phases and the number of diffusing components; in three-component models with some components precluded from diffusing, either by thermodynamic saturation (constant μ) or vanishingly small diffusion coefficients, the number of phases in a layer can be less than, equal to, or greater than the number of diffusing components. However, there is a clear tendency for natural, multicomponent sequences to have a limited number of minerals per layer (e.g. Brady, 1977). The next section shows that a correspondence exists between steady-state diffusion-control theory and Korzhinskii's rule, if 'perfectly mobile' components are incorporated in a simplified, limiting form of the theory. In later sections, a more realistic interpretation of the natural example will be compared with this limiting case.

Diffusion theory and perfectly mobile components

At local equilibrium, the diffusive flux of component i is related to the chemical-potential gradient $d\mu_i/dx$ by a diffusion coefficient L_{ii}:

$$J_i = -L_{ii}\frac{d\mu_i}{dx} \tag{1}$$

(cross-coefficients L_{ij}, $i \neq j$, are neglected). Following Joesten (1977), equation 1 for each component is combined with the Gibbs-Duhem equation for each mineral (modelled as a homogeneous phase). At constant pressure and temperature, the Gibbs-Duhem equation for phase k is

$$\sum_i n_i^k \, d\mu_i = 0 \tag{2}$$

where n_i^k is the number of moles of component i in phase k. Computer modelling uses ratios of L_{ii} to the L-coefficient of a reference component, here L_{SiSi} (Si is an abbreviation for SiO_2, since the modelling assumes oxide components). Then combining equations 1 and 2 gives

$$\sum_i n_i^k \, J_i \frac{L_{SiSi}}{L_{ii}} = 0 \tag{3}$$

for each phase in a given layer (the 'flux ratio equations' of Joesten, 1977, Appendix A). The mathematics can handle 'perfectly mobile' components (finite flux, zero μ-gradient) by setting their L_{ii} to infinity ($L_{SiSi}/L_{ii} = 0$). Other components will be called 'finitely mobile'.

Ashworth and Birdi (1990) showed that, given sufficient constraints from observations, the system of equations can be solved stepwise at each contact between layers. For a system with N components and ϕ phases altogether (including the reactants), the stoichiometric coefficients ν_k^q in the local reaction at a particular contact q, for phases present in the next layer, are found using summations over contacts up to q and over all ϕ phases:

$$\sum_{m=1}^{q} \sum_{l=1}^{\phi} A_{kl} \, \nu_l^m = 0 \tag{4}$$

where the A-coefficient links the effects of phases k and l,

$$A_{kl} = \sum_{i=1}^{N} n_i^k \, n_i^l \frac{L_{SiSi}}{L_{ii}} . \tag{5}$$

For example, at contact 1 (Pl|Hbl + Spl) of Ashworth and Birdi (1990), with the coefficient of plagioclase ν_{Pl}^1 set to unity, the equations to be solved for ν_{Hbl}^1 and ν_{Spl}^1 are:

$$\left.\begin{aligned} A_{HblHbl}\,\nu_{Hbl}^1 + A_{HblSpl}\nu_{Spl}^1 &= \\ &\quad -A_{HblPl} - A_{HblMet1} \\ A_{HblSpl}\,\nu_{Hbl}^1 + A_{SplSpl}\nu_{Spl}^1 &= \\ &\quad -A_{SplPl} - A_{SplMet1} \end{aligned}\right\} \tag{6}$$

where Met1 is a fictive phase to account for the metasomatic fluxes at contact 1 of an open system (Ashworth and Birdi, 1990). Now, there is a lower limit to the number of finitely mobile

components, N_F, in a viable model, due to the symmetrical array of A-coefficients on the left-hand sides of such equations. They have no solution (the determinant is zero) unless $N_F \geq \Phi$, where Φ is the number of phases in the layer. This is illustrated for the case $\Phi = 2$ by equations 6: the determinant is

$$A_{\mathrm{HblHbl}} A_{\mathrm{SplSpl}} - (A_{\mathrm{HblSpl}})^2$$

which is a summation over i and j of terms

$$(n_i^{\mathrm{Hbl}})^2 (n_j^{\mathrm{Spl}})^2 \frac{L_{\mathrm{SiSi}}}{L_{ii}} \frac{L_{\mathrm{SiSi}}}{L_{jj}} - n_i^{\mathrm{Hbl}} n_i^{\mathrm{Spl}} n_j^{\mathrm{Hbl}} n_j^{\mathrm{Spl}} \frac{L_{\mathrm{SiSi}}}{L_{ii}} \frac{L_{\mathrm{SiSi}}}{L_{jj}}.$$

Such a term is evidently zero if $i = j$. For the summation to have a finite value requires that some terms with $i \neq j$ are finite, which requires at least two non-zero L-ratios, i.e. at least two finitely mobile components. The restriction, $\Phi \leq N_F$, is the same as Korzhinskii's (1959) phase rule, if an 'inert' component is redefined as a 'finitely mobile' one (L_{ii} finite).

In the case of Ashworth and Birdi (1990), if Al and Si are the only two finitely mobile components, the correct layer sequence Pl|Hbl + Spl|Hbl|Opx|Ol can be generated. However, it is more realistic to regard all components as finitely mobile. The detailed fit obtained by Ashworth and Birdi (1990), reproducing the observed Hbl/Spl ratio in the two-phase layer, had Fe, Mg, Ca and Na finitely mobile but with larger L_{ii} than Al and Si. The low mobilities of Al and Si result in small fluxes: the two-mineral symplectite is produced at the Pl contact to accommodate an Al/Si ratio approximating that of reactant Pl. This result suggests a slight modification of Korzhinskii's concept, so that all components may be finitely mobile but the maximum number of minerals in a layer may be controlled by a set having lower mobilities than the others: $\Phi \leq N_R$, where N_R is the number of relatively immobile components. This is the idea that will be further explored below, for a 4-phase layer.

Geological setting

The sample studied in this paper (VW20) is from the Jotun Nappe Complex, Norway. The locality (grid reference 937 132) is a few km east of the area mapped by Emmett (1982, 1989), from which came the coronas between clinopyroxene and plagioclase studied by Ashworth *et al.* (1992). Sample VW20 is tentatively assigned to the Storådalen Complex of Emmett (1982), a unit of granoblastic orthogneisses of ultrabasic, basic and intermediate composition, metamorphosed prior to 1450 Ma under intermediate-pressure granulite-facies conditions (Corfu and Emmett, in preparation). The coronas are fine-scale (Fig. 1) and retrograde, with assemblages suggesting the epidote-amphibolite facies, as in the samples described by Ashworth *et al.* (1992). In the latter, the coronas probably formed during the Scandian (= late Caledonian) Orogeny (Ashworth *et al.*, 1992), when the Precambrian rocks were transported by thrusts to form the Nappe Complex. For the more complicated coronas studied here, an additional earlier stage of evolution is not ruled out.

Petrography

In addition to optical microscopy, the fine-grained coronas were also examined by electron-probe microanalysis, backscattered-electron (BSE) imaging in the scanning electron microscope, and analytical transmission electron microscopy (ATEM) of ion-thinned areas. Minerals are identified in ATEM by electron-diffraction patterns and X-ray emission spectra.

The major primary minerals are olivine (Ol) and plagioclase (Pl), with minor brown amphibole, orthopyroxene (Opx), green spinel (Spl) and opaques. The coronas studied in detail are consistently developed between Ol and Pl (Fig. 1*a*). The outer parts (near Pl) are similar to other coronas, separating Pl from primary amphibole and opaques.

Optically, the coronas between Ol and Pl show threefold layering (Fig. 1*b*). Next to Ol is a layer of Opx or talc. Talc irregularly penetrates olivine (which has also been largely serpentinised; Fig. 1*a*).

The second optical layer is brown and turbid in transmitted light. BSE and electron-probe work indicate a symplectite, of bulk composition consistent with amphibole + Spl. These two minerals are confirmed by ATEM (Fig. 1*f*). The symplectite is separated from Opx (or talc) by a narrow layer of amphibole.

The third optical layer (adjacent to Pl) is pale green and contains an optically resolved high-relief mineral (Fig. 1*b*). This mineral is bright in BSE images (Fig. 1*c*), and is identified from electron-probe data as epidote (Ep), intergrown with amphibole. Immediately adjacent to Pl, narrow dark bands in BSE (Fig. 1*c*) indicate a third mineral, identified by ATEM as kyanite (Ky; Fig. 1*d*). Further from Pl, ATEM shows Spl instead of kyanite with the Ep and amphibole. A further, minor mineral near the Ky-bearing layer

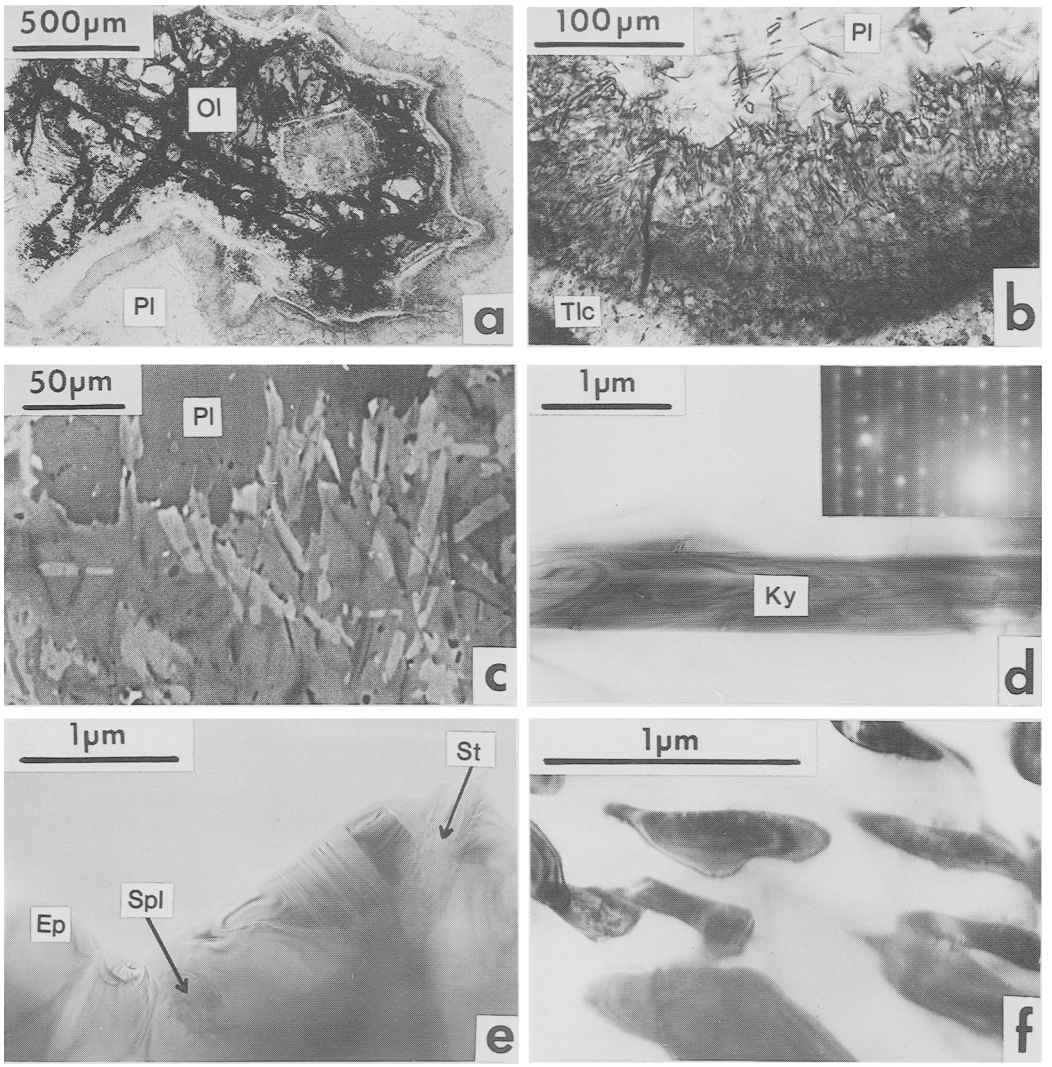

FIG. 1. Optical (*a,b*), BSE (*c*) and TEM (*d–f*) images of coronas in sample VW20. (*a*) Olivine (Ol, largely serpentinised) and plagioclase (Pl), separated by typical layered corona. Transmitted, plane polarised light. (*b*) Detail of corona showing elongate, high-relief epidote grains in and near Pl. A dark, turbid layer separates the epidote-bearing region from clear talc (Tlc). Transmitted, plane polarised light. (*c*) The layer adjacent to Pl with Ep distinguished in BSE contrast as brighter than coexisting amphibole. Narrow, dark bands are interpreted as kyanite from TEM evidence: (*d*) shows typical elongate kyanite, in amphibole, seen in TEM. The habit plane of kyanite is (100). Identification as Al_2SiO_5 is confirmed by X-ray emission spectra. The [001] diffraction pattern (inset) distinguishes the mineral from andalusite or sillimanite and also reveals (100) twinning. (*e*) Four-mineral assemblage revealed by TEM: amphibole contains epidote (Ep: only part of a relatively large grain is seen, with straight boundary), a bleb of spinel (Spl) and a lath of staurolite (St). Mineral identifications are confirmed by X-ray emission spectra and diffraction patterns. The featureless upper part of the field of view is a hole made by ion-thinning. (*f*) Fine-scale symplectite of spinel (dark, because in strongly diffracting orientation) in amphibole.

is staurolite (St; Fig. 1*e*). Ep, St and Spl form separate inclusions in the amphibole, but are closely adjacent and elongated in approximately the same direction, forming a symplectite-like intergrowth.

Using BSE images, layer widths were measured in traverses of one corona, and mineral proportions within layers were estimated as far as possible by digitising the photographs (Table 1). Ky and St, and Spl with amphibole + Ep + St, are

Table 1. Summary of corona petrography.

Layer minerals	Relative layer width	Mineral volume proportions	Bulk Al/Si atom ratio (by electron probe)
Amphibole (Ts) + Ep + Ky	1.178	Ep/(Ts + Ky) = 0.41 ± 0.06 (n = 5)	0.78 ± 0.10 (n = 13)
Amphibole + Ep + Spl (+ St near Ts+Ep+Ky)	0.513	Structure not fully resolved	
Hbl + Spl	0.662	Spl/Hbl = 0.33 ± 0.06 (n = 4)	0.74 ± 0.10 (n = 6)
Hbl	0.149	-	0.22 (n = 1)
Opx	1	-	-

n = number of measurements

present in too small proportion to be measured. ATEM does not give mineral proportions because the ion-thinned areas are too small to be reliably representative.

Mineral compositions

Wavelength-dispersive electron-probe analyses were obtained at 20 kV and 20–25 nA, using a Cameca Camebax instrument. Further data were obtained by ATEM, which is less precise, but necessary to resolve the intergrown minerals. A JEOL 4000FX instrument with Link Systems energy-dispersive X-ray detector was operated at 300–400 kV, and calibrated by powdered silicate standards from the British Museum (Natural History). Element ratios were estimated using the thin-film approximation (Lorimer and Cliff, 1976). Table 2 gives results recalculated to mineral formula units. Scatter in these data is largely attributable to counting statistics, though real variation is confirmed in amphibole and Spl.

In electron-probe data, Ol is homogeneous with composition Fo_{87}, and Opx is $En_{79\pm2}$. Good Pl analyses are An_{69-81} (Al/Si = 0.73–0.82), but Al/Si ratios up to 0.85 were recorded, probably due to small Ep inclusions (visible in Fig. 1*b*). Approximately the same bulk Al/Si is indicated by electron-probe analyses in the Ky-bearing and Spl-rich layers (Table 1). The complex region between these could not be reliably isolated in the probe work.

ATEM shows that the amphibole coexisting with Ep is highly aluminous (Table 2). Because Fe^{3+}/Fe^{2+} ratios and A-site occupancies cannot be determined by the methods used, the nomenclature is uncertain between tschermakite, pargasite and magnesio-hastingsite (Leake, 1978); but the amphibole clearly has a large proportion of the alumino-tschermakite end-member, and will be denoted by the abbreviation Ts. In the optically brown areas more distant from Pl, the amphibole is zoned to much lower Al contents (accompanied by higher Mg and Si). In the symplectite with Spl, this zoning is patchy, but Al is systematically low in the monomineralic layer. The lowest Al contents (Table 2), indicating actinolite, were found furthest from the symplectite (adjacent to talc). On average, the zoned amphibole can be termed hornblende (Hbl), as is confirmed by an electron-probe analysis of the monomineralic layer giving Si = 7.02. Spinel shows variation in Mg/Fe ratio, but no spatial pattern was noticed.

Table 2. Compositional data from ATEM.

	Amphibole: in Ep-bearing layers (n = 9)	Amphibole: without Ep (n = 8)	Ep (n = 9)	St (n = 2)	Spl (n = 10)
Recalculation basis:	15 cations excluding Na		16 cations (anhydrous)	23 oxygens (anhydrous)	18 cations
Na	0.51-0.94	0.38-0.93	-	-	-
Mg	2.17-2.97	2.95-4.65	0.19-0.31	0.84-1.07	1.89-4.57
Al	3.13-3.74	0.40-3.32	4.67-5.15	8.52-8.89	11.12-11.81
Si	5.74-6.09	5.76-7.70	5.82-6.11	3.83-3.92	-
Ca	1.83-2.07	1.71-2.12	3.75-4.07	0.03-0.04	-
Fe	1.05-1.44	0.54-1.06	0.70-0.98	1.12-1.28	1.88-4.98

n = number of analyses

Interpretation

Coexistence of staurolite or kyanite with calcic amphibole

These unusual mineral pairs have previously been described both from clearly high-pressure settings (Enami and Zang, 1988; Gil Ibarguchi *et al.*, 1991) and from amphibolites in regions of Barrovian metamorphism (Spear, 1982; Helms *et al.*, 1987). Staurolite inclusions in amphibole + Spl symplectite were described by Ward (1984). In all these occurrences, the amphibole has high Al and the staurolite has high Mg. In the extreme case of Enami and Zang (1988), Al = 3.65 in the amphibole formula and Mg/(Mg + Fe) = 0.68–0.74 in staurolite. The amphiboles in the present study are comparably aluminous; staurolite is less magnesian (Table 2), though Mg-rich compared to common staurolite in Barrovian pelites (e.g. Schumacher, 1985).

The amphibole + staurolite assemblages have been attributed to relatively high pressure, partly because pure Mg-staurolite is a high-P mineral (Schreyer, 1988), and also because the assemblages with St or Ky are thought to represent the high-P side of the reaction that can be written between St + Hbl + H_2O (or Ky + Hbl + H_2O) and the more common subassemblage Ep + Pl + garnet + chlorite + quartz (Selverstone *et al.*, 1984; Helms *et al.*, 1987). However, the presence of H_2O in the equations indicates that St + Hbl and Ky + Hbl should be favoured by water-undersaturated conditions (Grew and Sandiford, 1985). Absence of fluid phase is suggested by the small scale of corona reactions (cf. Ashworth and Birdi, 1990). Therefore the assemblages may have been stabilised by low μH_2O, and it is not necessary to invoke unusually high pressures.

Commonly in coronas around Ol, the layer next to Pl comprises Hbl + Spl (Ashworth and Birdi, 1990). In comparison, the Ts + Ep + Ky layer of the present example has very similar density, but is more hydrated and more oxidised, suggesting possibly lower-grade conditions.

Model phase compositions and overall equation

The diffusion modelling uses fixed compositions of minerals (treated as homogeneous phases) and requires that an overall corona-forming reaction be reconstructed (Ashworth and Birdi, 1990). The model phase compositions (Table 3) are based on 24 oxygens. Talc and serpentine are neglected as presumably representing selective hydration of Opx and Ol at a later stage, after the main corona-forming reaction.

Pl, Ol and Opx compositions are based on electron-probe data. Al/Si ratios will be important in the modelling. The model Pl is An_{80}, with Al/Si = 0.82, consistent with data for Pl containing Ep inclusions (cf. Ashworth *et al.*, 1992). Minor metasomatism of other components in Pl during inclusion formation should not affect the modelling of the corona. Other phase compositions are based on ATEM data (Table 2). In spinel, Fe^{3+} is calculated from stoichiometry; this is not feasible in Ep, where all Fe is treated as Fe^{3+}, and amphibole, where all Fe is treated as Fe^{2+} (Table 3). Modelling with two amphibole 'phases' (Ts and Hbl) is rather artificial in the presence of zoning, which indicates compositional evolution during growth (Ashworth *et al.*, 1992), as discussed below. The Hbl 'phase' in Table 3 is based on an ATEM analysis within the zoned amphibole, chosen to be consistent with the observed bulk Hbl/Spl and Al/Si ratios of the Hbl + Spl symplectite (Table 1).

Observed mineral proportions (Table 1, corrected from volume to molar terms using volume factors in Table 3) are used in constructing the overall equation. These data need to be supplemented by further considerations as follows. In the assemblage Ts + Ep + Ky the proportion of Ky is calculated from measured Ep/(Ts + Ky) and Al/Si ratios. Between this layer and Hbl + Spl is the incompletely characterised, complex region. Assuming that it has bulk Al/Si = 0.76, similar to the layers on either side, its mineral proportions can be calculated for assumed values of the ratios

Table 3. Model phase compositions (24-oxygen basis), and factors used to correct volume to molar proportions.

	Si	Al	Mg	Fe^{2+}	Fe^{3+}	Ca	Na	H	Volume factor
Pl	6.60	5.40	-	-	-	2.40	0.60	-	1.193
Ts	5.86	3.32	2.76	1.11	-	1.95	0.76	2.00	1.082
Ep	5.59	4.60	0.23	-	0.76	3.63	-	1.85	1.031
Ky	4.80	9.60	-	-	-	-	-	-	0.837
St	3.87	8.71	0.96	1.20	-	-	-	2.00	0.866
Spl	-	11.49	3.24	2.76	0.52	-	-	-	0.950
Hbl	7.13	1.02	4.41	0.54	-	1.90	0.42	2.00	1.082
Opx	7.75	0.44	6.17	1.63	-	0.04	-	-	1
Ol	6.00	-	10.44	1.56	-	-	-	-	1.046

Ep/Ts and St/Spl. Trial modelling at various reasonable values of these ratios showed that the outcome is insensitive to the variation; a value of 0.3 for both ratios has been used.

The system is assumed to be closed to $AlO_{3/2}$ and SiO_2, an assumption justified by the approximate local conservation of Al/Si ratio in the layers near Pl (cf. Ashworth and Birdi, 1990). The overall model reaction is then:

$$1\ \text{Pl} + 0.796\ \text{Ol} + 0.730\ \text{FeO} + 0.169\ \text{CaO} + 0.236\ \text{FeO}_{3/2} + 2.194\ \text{HO}_{1/2} \rightarrow 0.553\ \text{Ts} + 0.236\ \text{Ep} + 0.066\ \text{Ky} + 0.004\ \text{St} + 0.108\ \text{Spl} + 0.322\ \text{Hbl} + 0.540\ \text{Opx} + 1.622\ \text{MgO} + 0.044\ \text{NaO}_{1/2}. \quad (7)$$

This reaction has a solid volume change of approximately −7%.

Approach to diffusion modelling

Some further assumptions are necessary. Sensitivity of the modelling to assumed quantities will be assessed below. As in our previous studies (Ashworth and Birdi, 1990; Ashworth *et al.*, 1992), the assumption of closure to $AlO_{3/2}$ and SiO_2 has led to metasomatic exchange of other components between the corona-forming system and its surroundings (eqn. 7).

Modelling requires locations to be specified for these metasomatic fluxes. As in the coronas around olivine discussed in detail by Ashworth and Birdi (1990), it seems most likely that CaO and $NaO_{1/2}$ were exchanged at the Pl contact, other metasomatic fluxes (of Mg and Fe oxides) being accommodated at the Ol contact, largely by diffusion within Ol.

The presence of both Fe^{2+} and Fe^{3+} provides a further problem. Ashworth *et al.* (1992) noted that interconversion of these within a corona is likely. In the present case, Fe derived from Fe^{2+} in Ol is likely to be oxidised during diffusion, to produce the Fe^{3+} in Ep and Spl (Table 3). We have no constraints on the location of the oxidation reaction, and the simple assumption is made that all Fe^{3+} for production of Ep and Spl diffuses as Fe^{3+} throughout its transport.

In addition to the fixed phase compositions and product mineral proportions (defining the overall reaction), the inputs to the model are the L-ratios L_{SiSi}/L_{ii} that appear in equation 3, whose values are varied between computer runs. Following Joesten (1977) as discussed by Ashworth and Birdi (1990), it is assumed that these are constant throughout the corona. The component $HO_{1/2}$ is treated as perfectly mobile ($L_{SiSi}/L_{HH} = 0$). For other ratios, values were varied to find the range that reproduces the observed corona as well as possible.

The ideal outcome is to match exactly the actual mineral proportions in each layer (Ashworth and Birdi, 1990). The distribution of minerals is incompletely defined by the present data (Table 1), but the theory places limitations on the possible layer sequences, as follows. Except for one layer, which grows at both contacts, a layer grows at one contact and is consumed at the other (Fig. 2). Consider a layer B growing at the expense of layer A. If a phase that is present in A is also produced by the local

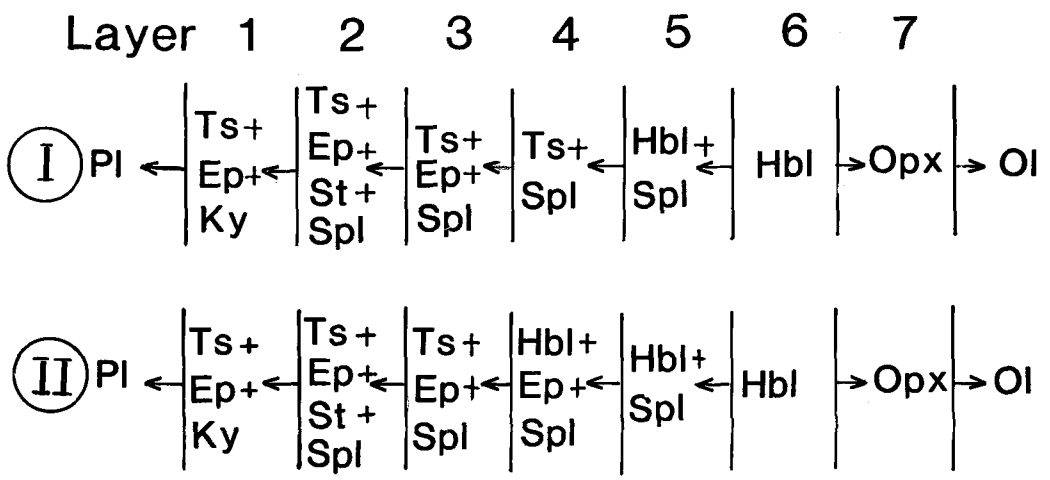

FIG. 2. Two hypothetical sequences of layers consistent with observation and with theoretical considerations. Arrows at contacts indicate the direction in which a layer is growing at the expense of the adjacent layer. In both layer-sequences, the unique layer growing at both its contacts is the hornblende layer, numbered 6.

reaction at the A|B contact, it remains present in B. In this case, the local reaction must also consume at least one phase that is present in A (Ashworth and Birdi, 1990, p. 2396). If more than one phase is consumed, all but one will be left in residual amounts and transferred across the contact into layer B (Joesten, 1977, p. 660), unless the L-ratios are specially related (so that two or more phases are consumed in exactly the proportion present in A). Therefore, in a 'bivariant field' of an L-ratio diagram (such as Fig. 3, discussed below), *exactly one phase is eliminated* between the retreating layer and the growing one. This rule is equivalent to those stated by Frantz and Mao (1975), and is satisfied by both layer sequences in Fig. 2. They are also consistent with the petrographic data (Table 1) and the treatment of amphibole as two phases Ts and Hbl. Considering all the observations, sequence I is a better fit than sequence II, because Al-poor amphibole (Hbl in the model) was not found with Ep in the ATEM survey (Table 2).

Modelling results

Like the coronas studied by Ashworth and Birdi (1990) and Ashworth *et al.* (1992), the present example is best modelled with some ratios $L_{ii}/L_{SiSi} > 1$ and also $> L_{AlAl}/L_{SiSi}$, i.e. Al and Si less mobile than some components i, as measured by diffusion coefficients L_{ii}. This is illustrated by diagrams showing stability fields of layer sequences (Fig. 3, in which L_{AlAl}/L_{SiSi} is held constant). Unlike the previous studies, the modelling does not produce a realistic result if all L_{ii}/L_{SiSi} ($i \neq$ Al) are held equal. In particular, $L_{Fe^{3+}Fe^{3+}}/L_{SiSi}$ and L_{CaCa}/L_{SiSi} must be relatively small in order to model the 4-phase layer Ts + Ep + St + Spl. Therefore, these two L-ratios are separated from others in constructing Fig. 3. The 4-phase layer places severe restrictions on the L-ratios: it has only a narrow band of stability, at low L_{CaCa}/L_{SiSi} and $L_{Fe^{3+}Fe^{3+}}/L_{SiSi}$ relative to the other variable in the calculations, L_{ii}/L_{SiSi} (i = Fe^{2+}, Mg, Na). Within this stability band, the full sequence computed is sequence II of Fig. 2. Sequence I, which would be preferable as a fit to observations, has no stability field. Instead, Fig. 3 shows a stability field for sequence Ia, which differs from I in having no 4-phase layer (Spl being absent from layer 2). Sequence IIa of Fig. 3 bears the same relation to sequence II.

The restrictions on stability of the 4-phase layer are insensitive to changing the locations of metasomatic fluxes from Pl to Ol or vice versa, and to likely errors ($\approx \pm 10\%$) in the overall product phase proportions (eqn. 7) or their compositions (Table 3). Trial calculations with oxidation of Fe^{2+} to Fe^{3+} during transport also indicated no important difference in the outcome of the modelling, as did introducing Fe^{3+} into phases in which treating all Fe as Fe^{2+} in Table 3 may be erroneous (notably amphiboles).

The boundary labelled 'no Hbl layer 6' in Fig. 3*a* refers to the disappearance of the monomineralic Hbl layer (numbered 6 in Fig. 2), and is analogous to an important boundary in the simpler case of Ashworth and Birdi (1990). The Hbl layer in mid-corona is not produced at small values of L_{ii}/L_{SiSi} ($i \neq$ Al), because the increasing mobility of Al relative to other components allows the Al-rich minerals to spread into this part of the corona. As in the case of Ashworth and Birdi (1990, Fig. 6), this boundary moves to larger L_{ii}/L_{SiSi} ($i \neq$ Al) with increasing L_{AlAl}/L_{SiSi}. Thus, if Fig. 3*a* was redrawn at larger L_{AlAl}/L_{SiSi}, stability fields Ia, IIa and II would be restricted to larger values of both plotted variables. There would be little effect on other aspects of Fig. 3*a*.

The other boundaries in Fig. 3*a* reflect the distribution of St, Ep and Spl among layers 2, 3 and 4. With increasing L_{CaCa}/L_{SiSi} and $L_{Fe^{3+}Fe^{3+}}/L_{SiSi}$, Ep disappears from layer 4 and then layer 3 (at each boundary of field Ia). This increasing restriction of Ep production to layers near the reactant Pl is also illustrated by the contours of Ep/(Ts + Ky) ratio in layer 1 (Fig. 3*a*). Both Fe^{3+} and Ca are major constituents of Ep. Fe^{3+} diffuses towards Pl (from an ultimate source as Fe^{2+} in Ol). Increasing $L_{Fe^{3+}Fe^{3+}}/L_{SiSi}$ facilitates this, promoting Ep production at the Pl contact. In computations at large L_{CaCa}/L_{SiSi}, Ca diffuses in the same direction, despite being ultimately sourced in Pl (i.e. it back-diffuses from contacts in mid-corona where Ca-rich minerals are consumed, like Mg in the case treated by Ashworth *et al.*, 1992). Then increasing L_{CaCa}/L_{SiSi} also promotes Ep production at Pl.

To match observation, the Ep/(Ts + Ky) ratio should be 0.41 ± 0.06 (Table 1; the correction from volume to molar proportions is negligible for this ratio). In Fig. 3, this condition is met in the ruled part of field II which therefore represents an acceptable model for layers 1 and 2 and the best model obtained for the corona as a whole, while field Ia remains a better fit for the Hbl-bearing part.

In Fig. 3*b*, L_{CaCa}/L_{SiSi} and $L_{Fe^{3+}Fe^{3+}}/L_{SiSi}$ are varied separately. The observed Ep/(Ts + Ky) ratio can be modelled at large L_{CaCa}/L_{SiSi} in field Ia, provided that $L_{Fe^{3+}Fe^{3+}}/L_{SiSi}$ is relatively small. This does not close the gap between fields II and Ia, i.e. does not tend to produce a stability field for the preferred sequence I. Nor could

complete agreement with observation be achieved by varying $L_{Fe^{2+}Fe^{2+}}$, L_{MgMg} and L_{NaNa} separately.

Table 4 shows numerical results for the local reactions, with a set of L-ratios lying in the stability field of sequence II in Fig. 3*b*. Ep is consumed at contacts 2 and 3 but is transferred in residual amounts across both. This feature of the modelling appears realistic; the residual Ep contributes to maintaining bulk Al/Si ratios close to that of model Pl (0.82) throughout the Pl-derived part of the corona (layers 1–5). These ratios (0.77–0.82) are within the uncertainties in the data (Table 1). The modelling gives bulk production ratios for layers 1 : (2 + 3 + 4) : 5 : 6 of 0.466 : 0.514 : 0.174 : 0.135, whereas the data give 0.611 : 0.263 : 0.341 : 0.075. The discrepancy in layer 6 could be eliminated by increasing L_{AlAl}/L_{SiSi} (spreading Hbl + Spl further towards Ol), but the other discrepancies cannot be eliminated. Essentially, in the model, layers 2 + 3 + 4 occupy too much space because Ep production is displaced more towards Ol than the data permit. This remains true in the modelling wherever the 4-phase layer Ts + Ep + St + Spl is stable.

Discussion

Possible sources of inadequacy in the model

The detailed differences between modelled and observed mineral distributions indicate that some of the assumptions in the modelling are invalid. A simple suggestion would be that L_{CaCa}/L_{SiSi} and $L_{Fe^{3+}Fe^{3+}}/L_{SiSi}$ were not constant, but were smaller in layers 1 and 2 than in layer 4, by about 1 order of magnitude (discrepancy between fields II and Ia in Fig. 3*a,b*). However, it may well be that the model is oversimplified in treating the zoned amphibole as two phases Ts and Hbl. Zoning indicates finite departure from the simple steady state with local equilibrium assumed in the modelling (cf. Ashworth *et al.*, 1992). In the present, complicated case, the data are insufficient to justify a more elaborate model. Although Ashworth *et al.* (1992) modelled a simple example of hornblende-actinolite zoning in terms of compositional evolution with local equilibrium maintained in grain boundaries, the present zoning from tschermakitic amphibole to actinolite is more extreme and may reflect further departure from equilibrium. The partial layer sequence near olivine, Hbl + Spl|Hbl|Opx, is more commonly found as a complete sequence between Pl and Ol (e.g. Ashworth and Birdi, 1990), and may represent an early corona on which the layers with Ts and Ep are a later overgrowth formed under different metamorphic conditions (e.g. lower T). In this case, Ol would continue to be a reactant but the early-formed corona would also be modified at the second stage. A changing reaction is difficult to reconstruct (cf. Carlson and Johnson, 1991), so the metasomatic fluxes are uncertain. However, to have a significant effect on the stability restrictions for the 4-phase layer, the metasomatic fluxes to be invoked at the Pl contact would be improbably large. The magnitudes can be gauged from Table 4: they would be required to eliminate the difference of an order of magnitude in fluxes through layer 2, between Ca, Fe^{3+}, Al, Si on the one hand and Mg, Fe^{2+} on the other. It is more likely that the model flux differences are realistic, and that the small fluxes of four components through the 4-phase layer have the thermodynamic connotation discussed in the following sections.

Immobile components and multiphase layers

In modelling of the present 4-phase assemblage (layer 2), large fluxes of Fe^{2+} and especially Mg through this layer are required by the reaction producing Ts in layer 1 (at the contact with Pl). Fe^{3+} is required in smaller amount for Ep, while Al, Si, and Ca are almost conserved in the reactions producing layers 1 and 2. It emerges from the computations that, for stability of the four-phase layer, these four components with small fluxes must also be relatively immobile in the sense of being assigned relatively small values of L_{ii}/L_{SiSi}. Because stability of the 4-phase layer is associated with immobility of four components, an analogy is suggested with the number N_I of 'inert' components in the phase rule $\Phi \leqslant N_I$ of Korzhinskii (1959).

Table 5 compares the twofold classification of components in Korzhinskii's (1959) theory with the cases arising in steady-state diffusion-control modelling. As indicated above in the section on diffusion theory, the latter certainly requires at least 4 finitely mobile components to model a 4-phase layer ($N_F \geqslant \Phi = 4$). In the limiting case $N_F = \Phi$, these components are fixed in the sense of having zero fluxes J_i (Table 5), as can be understood by examining Table 6. Here the substituted Gibbs-Duhem equation (eqn. 3) is written out for each of the phases in the present example. The components have been segregated in the equations, those modelled as relatively mobile being written on the right-hand side. If all of these are *perfectly* mobile (have $L_{SiSi}/L_{ii} = 0$), then the right-hand side of every equation is zero. Since all 4 components on the left are finitely mobile (have finite L-ratios), the only solution is

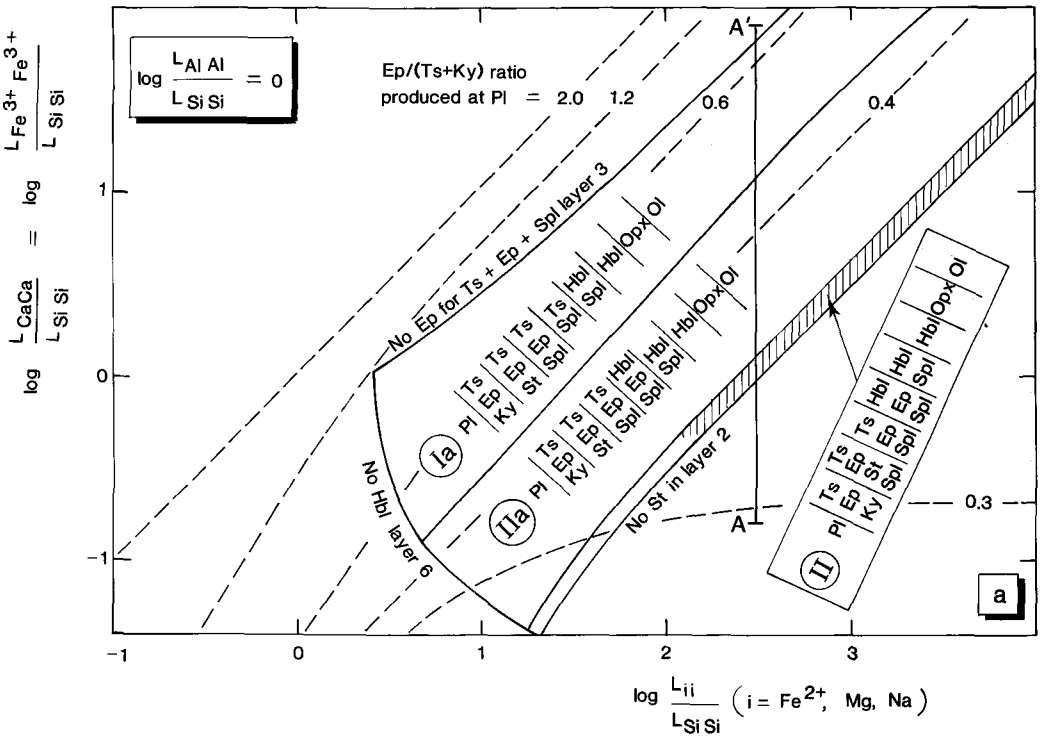
log L Fe3+ Fe3+ / L Si Si = log L CaCa / L Si Si
log L Al Al / L Si Si = 0
Ep/(Ts+Ky) ratio
produced at Pl = 2.0 1.2 0.6 0.4 0.3
No Ep for Ts + Ep + Spl layer 3
No Hbl layer 6
No St in layer 2
Ia
IIa
II
A
A'
a
log L ii / L Si Si (i = Fe2+, Mg, Na)

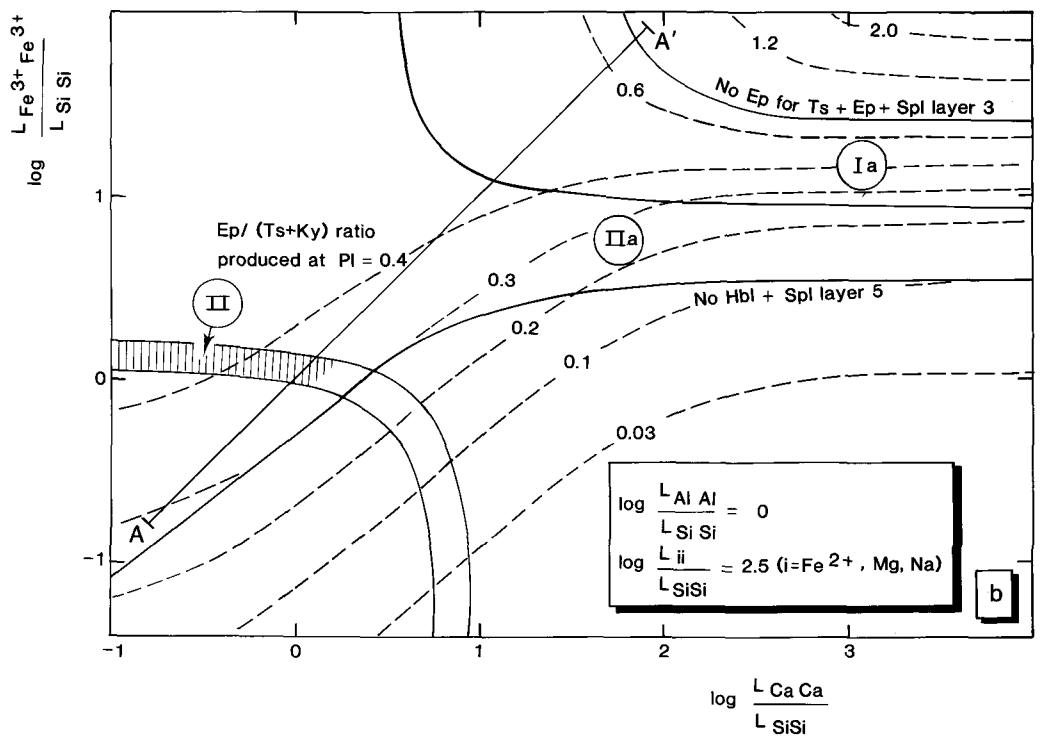
log L Fe3+ Fe3+ / L Si Si
Ep/ (Ts+Ky) ratio
produced at Pl = 0.4
2.0
1.2
0.6
0.3
0.2
0.1
0.03
No Ep for Ts + Ep + Spl layer 3
No Hbl + Spl layer 5
Ia
IIa
II
A
A'
log L Al Al / L Si Si = 0
log L ii / L SiSi = 2.5 (i=Fe2+, Mg, Na)
b
log L Ca Ca / L SiSi

Table 4. Typical numerical results of modelling, in the stability field of layer-sequence II (with 4-phase layer 2, Ts + Ep + St + Spl).

Input L-ratios:

i =	Al	Mg	Fe^{2+}	Fe^{3+}	Ca	Na	H
L_{ii}/L_{SiSi}	1.0	316	316	1.26	0.40	316	∞
$\log(L_{ii}/L_{SiSi})$	0	2.5	2.5	0.1	-0.4	2.5	∞

Coefficients of phases in the local reaction at each contact (negative if phase is produced):

Contact	Pl	Ts	Ep	Ky	St	Spl	Hbl	Opx	Ol
1	1.000	-0.670	-0.340	-0.166					
2		-0.073	0.038	0.101	-0.069	-0.026			
3		-0.086	0.045		0.065	-0.043			
4		0.276	-0.054			-0.042	-0.183		
5			0.074			-0.023	-0.070		
6						0.026	-0.005		
7							-0.064	0.075	
8								-0.615	0.795

Mineral content of each layer produced:

Layer	Ts	Ep	Ky	St	Spl	Hbl	Opx	Total	Al/Si
1	0.265	0.135	0.066					0.466	0.813
2	0.030	0.011		0.004	0.002			0.047	0.814
3	0.257	0.054			0.032			0.343	0.815
4		0.037			0.026	0.061		0.124	0.819
5					0.049	0.126		0.174	0.766
6						0.135		0.135	0.143
7							0.540	0.540	0.057

Ep/(Ts + Ky) in Layer 1 (produced at Pl) = 0.406
Spl/Hbl in Layer 5 = 0.387

Fluxes of components through each layer (negative if towards Pl):

Layer	Si	Al	Mg	Fe^{2+}	Fe^{3+}	Ca	Na	H
1	-0.027	0.013	-1.928	-0.744	-0.258	0.027	0.046	0.221
2	-0.023	0.011	-2.270	-0.980	-0.243	0.025	-0.009	0.008
3	-0.021	0.011	-2.573	-1.115	-0.230	0.022	-0.074	0.055
4	-0.008	0.014	-2.765	-1.022	-0.293	0.018	0.058	0.142
5	-0.097	0.013	-3.135	-1.125	-0.249	0.152	0.029	0.137
6	-0.133	0.303	-3.073	-1.057	-0.236	0.143	0.027	0.127
7	-0.008	0.270	-2.893	-0.969	-0.236	0.025	0.000	0.000

Metasomatic fluxes at contacts 1 and 8 (positive if influx):

Contact	Si	Al	Mg	Fe^{2+}	Fe^{3+}	Ca	Na	H
1	0.000	0.000	0.000	0.000	0.000	0.168	-0.045	2.190
8	0.000	0.000	-1.616	0.731	0.236	0.000	0.000	0.000

then $J_{Al} = J_{Si} = J_{Ca} = J_{Fe^{3+}} = 0$. Thermodynamically, the variance is zero so the μ-gradients are zero (Table 5), and therefore the fluxes are zero by equation 1.

The best fits to the data obtained above are similar to, but not identical with, the case $N_F = \Phi = 4$. More realistically, finite L_{SiSi}/L_{ii} values have been assigned to all components (except $HO_{1/2}$, which too could have been given a finite L_{SiSi}/L_{HH} without affecting the interpretation). The result can be viewed as a modification of the case $N_F = \Phi$, as follows. When non-zero L_{SiSi}/L_{ii} values are assigned to Mg and Fe^{2+}, their combination with the large J_i values produces non-negligible terms on the right of Table 6. Simultaneously the fluxes on the left-hand side become non-zero but remain

FIG. 3. Diagrams summarising the results of computer modelling of the coronas. The overall mineral proportions in the whole corona are fixed, but the distribution of these minerals among layers varies as the L-ratios (ratios of diffusion coefficients, L_{ii}/L_{SiSi}) are varied. In both diagrams, L_{AlAl}/L_{SiSi} is held constant (=1). Logarithms to the base 10 of other L-ratios are plotted. Stability fields are shown for the layer-sequences labelled Ia, II and IIa; for each of these, the minerals present in each layer are written on diagram (*a*). Also shown are contours of the ratio Ep/(Ts + Ky) produced in layer 1 by its growth from reactant Pl. The ruled area of stability field II represents the best approximation to the observed coronas. In (*a*), L_{CaCa}/L_{SiSi} and $L_{Fe^{3+}Fe^{3+}}/L_{SiSi}$ are held equal, whereas in (*b*) they are separately varied at a constant value of $10^{2.5}$ for $L_{Fe^{2+}Fe^{2+}}/L_{SiSi}$, L_{MgMg}/L_{SiSi} and L_{NaNa}/L_{SiSi}. Line A–A′ is the same in both diagrams.

Table 5. Comparison of classifications of components.

Source of theory: nomenclature of components; and constraint on number of phases ϕ	Diffusion coefficient L_{ii}	μ-gradient $d\mu_i/dx$	Flux J_i
Following Korzhinskii (1959):			
N_I inert components; $\phi \leq N_I$	not considered	finite	zero or small
perfectly mobile components	not considered	zero	finite
This work, based on Joesten (1977):			
N_F finitely mobile components; $\phi \leq N_F$			
(a) hypothetical limiting case $\phi = N_F$			
N_F finitely mobile components	finite	zero	zero
perfectly mobile components	infinite	zero	finite
(b) real case $\phi < N_F$;			
subdivision of finitely mobile components if N_R form a distinct, relatively immobile set			
N_R relatively immobile components; $\phi \leq N_R$	small	finite	small
relatively mobile components	large	finite	large

Table 6. Substituted Gibbs-Duhem equations (eqn. 3) for the four coexisting phases Ts + Ep + St + Spl, using compositional quantities n_i^k from Table 3, and with components separated into those inferred to be relatively immobile and those modelled as relatively mobile.

Phase	Left hand side: terms for relatively immobile components	
Ts:	$5.86\ J_{Si} + 3.32\ J_{Al}\frac{L_{SiSi}}{L_{AlAl}} + 1.95\ J_{Ca}\frac{L_{SiSi}}{L_{CaCa}}$	$= \ldots$
Ep:	$5.59\ J_{Si} + 4.60\ J_{Al}\frac{L_{SiSi}}{L_{AlAl}} + 0.76\ J_{Fe^{3+}}\frac{L_{SiSi}}{L_{Fe^{3+}Fe^{3+}}} + 3.63\ J_{Ca}\frac{L_{SiSi}}{L_{CaCa}}$	$= \ldots$
St:	$3.87\ J_{Si} + 8.71\ J_{Al}\frac{L_{SiSi}}{L_{AlAl}}$	$= \ldots$
Spl:	$11.49\ J_{Al}\frac{L_{SiSi}}{L_{AlAl}} + 0.52\ J_{Fe^{3+}}\frac{L_{SiSi}}{L_{Fe^{3+}Fe^{3+}}}$	$= \ldots$

Right hand side: terms for relatively mobile components				
$\ldots$	$- 2.76\ J_{Mg}\frac{L_{SiSi}}{L_{MgMg}}$	$- 1.11\ J_{Fe^{2+}}\frac{L_{SiSi}}{L_{Fe^{2+}Fe^{2+}}}$	$- 0.76\ J_{Na}\frac{L_{SiSi}}{L_{NaNa}}$	$- 2.00\ J_{H}\frac{L_{SiSi}}{L_{HH}}$
$\ldots$	$- 0.23\ J_{Mg}\frac{L_{SiSi}}{L_{MgMg}}$			$- 1.85\ J_{H}\frac{L_{SiSi}}{L_{HH}}$
$\ldots$	$- 0.96\ J_{Mg}\frac{L_{SiSi}}{L_{MgMg}}$	$- 1.20\ J_{Fe^{2+}}\frac{L_{SiSi}}{L_{Fe^{2+}Fe^{2+}}}$		$- 2.00\ J_{H}\frac{L_{SiSi}}{L_{HH}}$
$\ldots$	$- 3.24\ J_{Mg}\frac{L_{SiSi}}{L_{MgMg}}$	$- 2.76\ J_{Fe^{2+}}\frac{L_{SiSi}}{L_{Fe^{2+}Fe^{2+}}}$		

relatively small, so that balancing the equations requires relatively large L_{SiSi}/L_{ii} values on the left. The effect is illustrated graphically in Fig. 4. Two categories of component are recognisable, corresponding to (i) perfectly mobile and (ii) finitely mobile categories of the simplified case $N_F = \Phi$. These are (i) a set (Mg, Fe^{2+}) with large fluxes and high mobilities i.e. relatively large

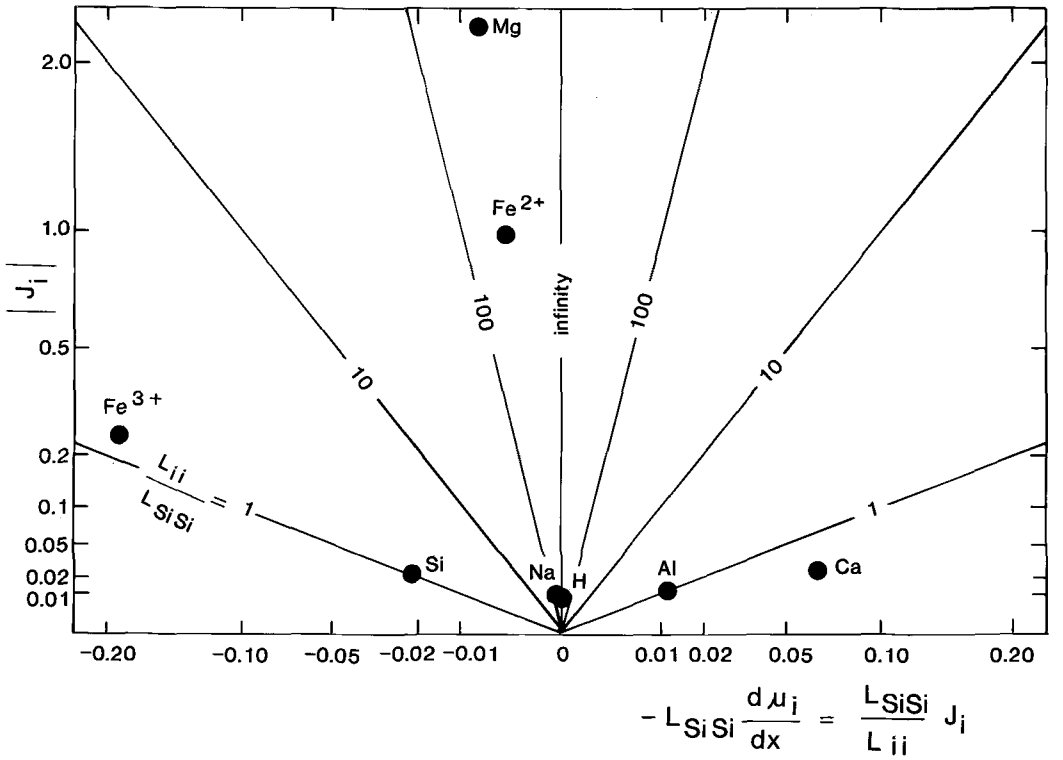

FIG. 4. Illustration of the distinction between (i) relatively mobile components (here Mg and Fe^{2+}), with large flux magnitudes $|J_i|$ and large diffusion coefficients L_{ii}, and (ii) relatively immobile ones (here Fe^{3+}, Si, Al and Ca) with small flux magnitudes and small L_{ii}. These contrasting behaviours are necessary for successful modelling of the 4-phase layer Ts + Ep + St + Spl; the results plotted are those of the example of modelling represented in Table 4 (layer 2). The non-linear (square root) scaling is used merely for clarity (to reduce the distances from the origin of the furthest points, relative to those of the nearest points). Components diffusing towards and away from Pl plot, respectively, to left and right of centre. The horizontal axis gives a measure of chemical-potential gradient. This quantity, multiplied by the composition factor n_i^k for phase k, must sum to zero over all components i to satisfy the Gibbs-Duhem equation for phase k, given in Table 6. The leftward and rightward-plotting components are so poised that this condition is satisfied for all 4 phases in the layer. In the example plotted, Na and H have small chemical-potential gradients because they have been assigned large diffusion coefficients L_{NaNa} and L_{HH}; they could be given small L-coefficients (leading to smaller $|J_{Na}|$ and $|J_H|$) without materially affecting the rest of the plot.

L_{ii}/L_{SiSi}, and (ii) a set (Fe^{3+}, Si, Al, Ca) with small fluxes and low mobilities, these being the N_R 'relatively immobile' components of Table 5. This classification is ambiguous for H and Na, which have small fluxes but are modelled with high mobilities (Fig. 4). They could equally well be modelled with lower mobilities, increasing the number of N_R of relatively immobile components: the condition $\Phi \leqslant N_R$ would still be obeyed.

Low mobility here implies difficulty of diffusion in grain boundaries which are probably solid (fluid-absent). Though faster than intracrystalline diffusion, this should have a similar mechanism. The commonly inferred relative immobility of Si^{4+} and Al^{3+} (Ashworth and Birdi, 1990) may be explained by the high charges on these cations (Dowty, 1980). The same reasoning applies to Fe^{3+}. Of the divalent cations under consideration, Ca^{2+} is the largest. There is evidence that intracrystalline diffusion is hindered by increasing ionic size (Dowty, 1980). Experimental evidence of relatively slow Ca diffusion in olivine has been attributed to this effect by Morioka (1981). It thus seems possible that, despite the more open and disordered structure of grain boundaries than crystal interiors, the behaviour of Ca in the reaction studied may be a size effect. However, in some other corona-forming reactions, there is no evidence for Ca and Fe^{3+} immobility (Ashworth *et al.*, 1992). Using Fig. 3, not for quantitative interpretation (in view of the uncertainties) but as

a general indication of behaviour, the present coronas with unusual multimineralic layers seem to represent conditions within a narrow band of L-ratios at unusually low L_{CaCa}/L_{SiSi} and $L_{Fe^{3+}Fe^{3+}}/L_{SiSi}$ relative to other L_{il}/L_{SiSi}. This difference from other coronas may reflect different metamorphic conditions, perhaps lower T or lower μH_2O.

Conclusions

The theory of steady-state diffusion-controlled growth, with local equilibrium, accounts for many but not all of the observed features of the complex coronas in sample VW20. The observations are consistent with a sequence of layer assemblages that would be permited by the theory (Fig. 2), but computations of the quantitative distribution of phases are inconsistent with the data. Also the observed amphibole is strongly zoned, indicating a departure from equilibrium which cannot be modelled, and suggesting that some of the complexity may be due to two-stage growth. Then the second stage, producing fairly homogeneous tschermakitic amphibole near Pl, with Ep + Ky in one layer and with Ep + St + Spl in the next, can be modelled with local equilibrium, in a restricted band of L-ratio values. There is some uncertainty about metasomatic fluxes at the Pl contact, but rather robust indication of relatively immobile behaviour of at least 4 components (i.e. $N_R \geq 4 \geq \Phi$). Two of these are Al and Si which, as in the coronas studied by Ashworth and Birdi (1990) and Ashworth *et al.* (1992), have small fluxes leading to approximate conservation of Al/Si ratios in layers near Pl. The other two are Ca and Fe^{3+}, whose low mobilities are also consistent with expected behaviour in fluid-absent grain-boundary diffusion.

The twofold subdivision of finitely mobile components in this study depends on N_R of them having *both* small fluxes and relatively small diffusion coefficients (Table 5). This allies their behaviour closely to that in the limiting, approximate model where *only* these few are treated as finitely mobile components. In other examples there might be no clear subdivision of the real, finitely mobile components, leaving only the weak constraint that Φ cannot exceed their (usually rather large) number N_F. However, it is obvious that the combination of small flux with small diffusion coefficient should be commonplace: from equation 1, it is expected wherever the μ-gradients of the various components are comparable. Therefore, it is suggested that the behaviour exemplified here may be rather general: in diffusion metasomatism approximating local equilibrium, there are few minerals per layer if there are few relatively immobile components, in the sense defined above.

Acknowledgements

Sample VW20 was collected by Vanessa Whelton while working with T.F.E. as supervisor; both acknowledge financial support from Anglia Higher Education College. J.J.B. acknowledges a NERC research studentship. We are grateful for facilities at the University of Edinburgh (electron probe, Dr P. Hill), and in the School of Metallurgy & Materials, University of Birmingham (SEM, Dr M. G. Hall, and ATEM, Prof. M. H. Loretto).

References

Ashworth, J. R. and Birdi, J. J. (1990) Diffusion modelling of coronas around olivine in an open system. *Geochim. Cosmochim. Acta,* **54**, 2389–401.

——— and Emmett, T. F. (1992) Diffusion in coronas around clinopyroxene: modelling with local equilibrium and steady state, and a non-steady-state modification to account for zoned actinolite-hornblende. *Contrib. Mineral. Petrol.*, **109**, 307–25.

Brady, J. B. (1977) Metasomatic zones in metamorphic rocks. *Geochim. Cosmochim. Acta,* **41**, 113–25.

Carlson, W. D. and Johnson, C. D. (1991) Coronal reaction textures in garnet amphibolites of the Llano Uplift. *Am. Mineral.*, **76**, 756–72.

Dowty, E. (1980) Crystal-chemical factors affecting the mobility of ions in minerals. Ibid. **65**, 174–82.

Emmett, T. F. (1982) Structure and petrology of the Bergen-Jotun kindred rocks from the Gjendebu region, Jotunheimen, central southern Norway. *Norges Geol. Unders.*, **373**, 1–32.

——(1989) Basic igneous rocks from a portion of the Jotun Nappe: evidence for Late Precambrian ensialic extension of Baltoscandia? In *The Caledonide Geology of Scandinavia* (R. A. Gayer, ed.). Graham & Trotman, London, pp. 143–51.

Enami, M. and Zang, Q. (1988) Magnesian staurolite in garnet-corundum rocks and eclogite from the Donghai district, Jiangsu province, east China. *Am. Mineral.*, **73**, 48–56.

Frantz, J. D. and Mao, H. K. (1975) Bimetasomatism resulting from intergranular diffusion: multimineralic zone sequences. *Carnegie Inst. Washington Yearb.*, **74**, 417–24.

———(1979) Bimetasomatism resulting from intergranular diffusion: II. Prediction of multimineralic zone sequences. *Am. J. Sci.*, **279**, 302–23.

Gil Ibarguchi, J. I., Mendia, M., and Girardeau, J. (1991) Mg- and Cr-rich staurolite and Cr-rich kyanite in high-pressure ultrabasic rocks (Cabo Ortegal, northwestern Spain). *Am. Mineral.*, **76**, 501–11.

Grant, S. M. (1988) Diffusion models for corona formation in metagabbros from the western Grenville Province, Canada. *Contrib. Mineral. Petrol.*, **98**, 49–63.

Grew, E. S. and Sandiford, M. (1985) Staurolite in a

garnet-hornblende-biotite schist from the Lanterman Range, northern Victoria Land, Antarctica. *Neues Jahrb. Mineral. Mh.*, 396–410.

Helms, T. S., McSween, H. Y. Jr, Labotka, T. C., and Jarosewich, E. (1987) Petrology of a Georgia Blue Ridge amphibolite unit with hornblende + gedrite + kyanite + staurolite. *Am. Mineral.*, **72**, 1086–96.

Joesten, R. (1977) Evolution of mineral assemblage zoning in diffusion metasomatism. *Geochim. Cosmochim. Acta,* **41**, 649–70.

——(1991) Local equilibrium in metasomatic processes revisited: Diffusion-controlled growth of chert nodule reaction rims in dolomite. *Am. Mineral.*, **76**, 743–55.

Johnson, C. D. and Carlson, W. D. (1990) The origin of olivine-plagioclase coronas in metagabbros from the Adirondack Mountains, New York. *J. Metamorphic Geol.*, **8**, 697–717.

Korzhinskii, D. S. (1959) *Physicochemical Basis of the Analysis of the Paragenesis of Minerals.* Consultants Bureau, New York.

Kretz, R. (1983) Symbols for rock-forming minerals. *Am. Mineral.*, **68**, 277–9.

Leake, B. E. (1978) Nomenclature of amphiboles. *Mineral. Mag.*, **42**, 533–63.

Lorimer, G. W. and Cliff, G. (1976) Analytical electron microscopy of minerals. In *Electron Microscopy in Mineralogy* (H.-R. Wenk, ed.). Springer-Verlag, Berlin etc., pp. 506–19.

Morioka, M. (1981) Cation diffusion in olivine—II. Ni-Mg, Mn-Mg, Mg and Ca. *Geochim. Cosmochim. Acta,* **45**, 1573–80.

Schreyer, W. (1988) Experimental studies on metamorphism of crustal rocks under mantle pressures. *Mineral. Mag.*, **52**, 1–26.

Schumacher, R. (1985) Zincian staurolite in Glen Doll, Scotland. Ibid., **49**, 561–71.

Selverstone, J., Spear, F. S., Franz, G. and Morteani, G. (1984) High-pressure metamorphism in the SW Tauern Window, Austria: *P–T* paths from hornblende-kyanite-staurolite schists. *J. Petrol.*, **25**, 501–31.

Spear, F. S. (1982) Phase equilibria of amphibolites from the Post Pond Volcanics, Mt Cube Quadrangle, Vermont. Ibid., **23**, 383–426.

Thompson, J. B., Jr (1970) Geochemical reaction and open systems. *Geochim. Cosmochim. Acta,* **34**, 529–51.

Ward, C. M. (1984) Magnesium staurolite and green chromian staurolite from Fiordland, New Zealand. *Am. Mineral.*, **69**, 531–40.

[*Manuscript received 16 August 1991: revised 20 February 1992*]